Journal of Molecular Structure 1217 (2020) 128327

Contents lists available at ScienceDirect

Journal of Molecular Structure

journal homepage: http://www.elsevier.com/locate/molstruc

Ruthenium (II) quinoline-azoimine complex: Synthesis, crystalline structures spectroelectrochemistry and catalytic properties

Mousa Al-Noaimi [a, *], Firas F. Awwadi [b, **], Ayman Hammoudeh [c], Obadah S. Abdel-Rahman [d], Manal I. Alwahsh [b]

[a] Department of Chemistry, Hashemite University, P.O.Box 150459, Zarqa, 13115, Jordan
[b] Department of Chemistry, The University of Jordan, Amman, 11942, Jordan
[c] Department of Chemistry, Yarmouk University, P.O. Box 566, Irbid, Jordan
[d] Department of Chemistry, College of Science, King Faisal University, PO Box 400, Hofuf, 31982, Saudi Arabia

ARTICLE INFO

Article history:
Received 14 March 2020
Received in revised form
20 April 2020
Accepted 23 April 2020
Available online 5 May 2020

Keywords:
Ruthenium
Quinoline -azoimine
Skeletal isomer
Spectroelctrochemistry
DFT calculation

ABSTRACT

An octahedral ruthenium(II) complex with the general formula $[Ru^{II}(Y)(bpy)Cl](ClO_4)$ {Y= $C_6H_5N{=}C(COCH_3)$-N=NC_9H_6N and bpy = 2,2′-bipyrdine} (**1**) was synthesized. The new ligand (Y) is coordinated to ruthenium via quinoline-N, imine-N and azo-N atoms. Both the novel complex **1** and the new ligand **H_2Y** were structurally characterized by X-ray crystallography, spectroscopic (IR, UV−Vis and NMR spectroscopy) and electrochemical (cyclic voltammetry) techniques. The bonding in **1** and its published skeletal isomer $[Ru^{II}(L1)(bpy)Cl](PF_6)$ {L1 = $C_6H_5N{=}N$-$C(COCH_3)$ = NC_9H_6N5} (**1A**) has been analyzed using molecular orbital theory. The novel tridentate ligand (Y) stabilizes the Ru(II) oxidation state showing the Ru(III/II) couple at 1.05 V vs. Cp_2Fe/Cp_2Fe^+. The potential use of **1** as a catalyst for hydrogenation of α, β-unsaturated aldehyde has been investigated. UV/Vis and IR-spectroelectrochemistry on complex 1 were performed.

CRedit author statement

Mousa Al-Noaimi: Conceptualization, Methodology, Funding acquisition, Formal analysis, Writing - original draft, Writing - review & editing, Approval of the version of the manuscript to be published. Firas F. Awwadi: Conceptualization, Methodology, Funding acquisition, Formal analysis, Writing - original draft, Writing - review & editing, Approval of the version of the manuscript to be published. Ayman Hammoudeh: Conceptualization, Methodology, Funding acquisition, Formal analysis, Writing - original draft, Writing - review & editing, Approval of the version of the manuscript to be published. Obadah S. Abdel-Rahman: Funding acquisition, Formal analysis, Approval of the version of the manuscript to be published. Manal I. Alwahsh: Funding acquisition, Formal analysis, Approval of the version of the manuscript to be published

1. Introduction

Pincer ligands (*mer*-tridentate ligand) are widely used in coordination chemistry because of their high thermal stability, chelating effect, high tunability, ability to coordinate a large variety of metals, and their application as homogeneous catalysis [1]. Moreover, the multiple synthetic approaches to tune the steric and electronic properties of these complexes to achieve the targeted applications have were applied, via the modification of the central coordinating atom, the lateral ones, and the linker between them [2]. A wide variety of NNO [3], NNP [4], NNS [5] and NHC-based pincer complexes [6] have found numerous applications in homogeneous catalysis and supramolecular chemistry. NNN pincer chelate ligand such as terpyridine derivatives play a fundamental role in inorganic chemistry [7].

8-Aminoquinoline and its derivatives have received much attention due to their medicinal properties [8,9]. They have been also used as strongly fluorescent ligands, chelates for heavy metals [10–12] and conducting co-polymers [13–16]. Because of the interesting properties of these materials, various synthetic routes have been developed to functionalize 8-Aminoquinoline by reacting it with carbonyl derivatives [17,18] or hydrazonylchloride [19] to

* Corresponding author.
** Corresponding author.
E-mail address: manoaimi@hu.edu.jo (M. Al-Noaimi).

https://doi.org/10.1016/j.molstruc.2020.128327
0022-2860/

produce pincer ligands analogous to terpyridine derivatives. Ruthenium complexes built from these ligands have been the foci for many research groups [20] as they can be used as hydrogenation, oxidation and polymerization catalysts [21–23].

Flexible polydentate azoimine (N=N-C=N-) ligands can be prepared by reacting hydrazonylchloride and amine derivatives [19,24–27]. Previously, we reported the synthesis of $[Ru^{II}(L1)(bpy)Cl](PF_6)$ { L1 = C_6H_5N=N-C($COCH_3$) = NC_9H_6N} (1A) where L1 is azoimine–quinoline pincer tridentate ligand which was prepared by reacting hydrazonylchloride with 8-aminoquinoline [19]. Herein, a new isomer of (H_2L) ligand namely quinoline -azoimine (H_2Y), was prepared by reacting 8-aminoquinoline hydrazonylchloride with aniline. A new octahedral ruthenium(II) complex having the general molecular formula $[Ru^{II}(Y)(bpy)Cl](ClO_4)$ (**1**) {bpy = 2,2′-bipyrdine and the new ligand (Y= C_6H_5N=C($COCH_3$)-N=HNC_9H_6N) has been synthesized to compare its structure and reactivity with the related complex **1A** reported previously (Scheme 1) [19]. The characterization of the complex was accomplished by X-ray diffraction as well as by a variety of spectroscopic techniques (IR, UV–Vis, ^{1}H, ^{13}C NMR, UV/Vis and IR-spectroelectrochemistry), in addition to cyclic voltammetric measurements. Furthermore, the synthesized complex has been tested as a catalyst for the hydrogenation of cinnamaldehyde in isopropanol in presence of KOH as a base.

2. Experimental

2.1. Chemicals and reagents

Ruthenium trichloride trihydrate, aniline, 3-chloro-pentane-2,4-dione, sodium nitrite, pyridine, 8-aminoquinoline and triethylamine were purchased from Aldrich and used without further purification. All solvents: diethyl ether (anhydrous, 99.0%), dichloromethane, acetone and absolute ethanol were purchased from TEDIA. 8-Aminoquinoline hydrazonylchloride was prepared according to published procedure [27].

2.2. Synthesis

2.2.1. ((1Z)-2-oxo-N-quinolin-8-ylpropanehydrazonoyl chloride

Yield. (3.2 g, 52%). Anal. Calc. for $C_{12}H_{10}N_3OCl$: C, 58.19; H, 4.07; N, 16.97. Found: C,58.21; H, 4.01; N, 16.71%. UV–Vis in acetonitrile: λ_{max} (ε_{max}/$M^{-1}cm^{-1}$): 368 (8.09×10^4), 276 (4.69×10^4), 254 (6.24×10^4). IR: ν(C=O) 1668, ν(C=N) 1577, ^{1}H NMR (DMSO, δ ppm): 10.53 (s, 1H, NH), 8.85 (d, 1H, H1), 8.10 (d, 1H, H6), 7.73 (d, 1H, H4), 7.55 (t, 1H, H5), 7.47 (m, 2H, H3, H2), 2.61 (s, 3H, $COCH_3$). ^{13}C NMR (DMSO, δ ppm):25.0 ($CO\underline{C}H_3$), 188.7 $COCH_3$, M.p is 130 °C.

2.2.2. Preparation and characterization of ((1Z)-2-oxo-N-quinolin-8-ylpropanehydrazonoyl chloride (H_2Y)

To a solution of (1Z)-2-oxo-N- quinoline -8-ylpropanehydrazonoyl chloride (4.94 g, 20 mmol) in 10.0 mL absolute ethanol, (1.84 g, 20 mmol) aniline and (2.4 g, 24 mmol) triethylamine were added. The mixture was refluxed for 2 h, a yellow solid was formed upon cooling to room temperature. The solid was recrystallized from ethanol yielding (3.6 g, 59%). Anal. Calc. for $C_{18}H_{16}N_4O$: C, 71.04; H, 5.30; N, 18.41, Found: C,71.21; H, 5.20; N, 18.31%. UV–Vis in acetonitrile: λ_{max} (ε_{max}/$M^{-1}cm^{-1}$): 368 (8.5×10^4), 276 (4.88×10^4), 254 (6.3×10^4). IR: ν(C=N) 1580, ν(C=O) 1660. ^{1}H NMR (DMSO, δ ppm): 9.42 (s, 1H, NH, 8.47 (s, 1H, NH), 8.10 (d, 1H, H6), 7.76 (d, 1H, H1), 7.55 (t, 1H, H5), 7.3 (m, 5H, H7, H8, H2), 6.95 (m, 2H, H9, H4), 6.79 (d, 1H, H3), 2.71 (s, 3H, $COCH_3$). M.p is 154 °C.

2.2.3. Preparation of [Ru(bpy)(Y)Cl]ClO_4(**1**)

(261 mg, 1.0 mmol) ruthenium trichloride trihydrate and (0.304 g, 1.0 mmol) of (H_2Y) were dissolved in 100 mL absolute ethanol. The mixture was refluxed for 2 h, then 1.0 mmol, 0.156 g) of 2,2′-bipyridine was added. The mixture was heated for an additional 1 h before an excess amount of LiCl (500 mg, 11.8 mmol) was added. The volume was reduced to 10 mL and then an excess of saturated aqueous solution of NH_4ClO_4 was added to precipitate the crude product. The crude product was filtered, washed with H_2O, diethylether, then dissolved in 20 mL (2:1) dichloromethane/acetonitrile and purified by chromatography on grade (III) alumina. The first yellow band, which corresponds to the ligand, was eluted with dichloromethane. The red band, which corresponds to the complex, is eluted with (1:1) dichloromethane: acetonitrile. Yield: (0.313 g, 45%). Anal. Calc. for $C_{28}H_{22}N_6O_5Cl_2Ru$: C, 48.42; H, 3.19; N, 12.10%. Found: C, 42.41; H, 3.42; N, 12.15%. UV–Vis in dichloromethane: λ_{max} in nm (ε_{max}/$M^{-1}cm^{-1}$): 242 (6.5×10^4), 300 (4.8×10^4), 360 (2.4×10^4), 410 (2.2×10^4), 502 (1.6×10^4). IR (cm^{-1}): ν(N=N) 1473, ν(C=N) 1605, ν(C=O) 1707. ^{1}H NMR (DMSO, δ ppm): 9.56 (t, 2H, H8), 8.57 (t, 1H, H9), 8.42 (d, 2H, H7), 8.18 (t, 1H, H5), 8.04 (t, 1H, H2), 7.95 (m, 2H, H1, H10), 7.68 (t, 1H, H11), 7.44 (m, 1H, H12) 7.20 (m, 2H, H13, H3), 7.20 (d, 1H, H6), 7.09 (t, 1H, H15), 6.99 (m, 2H, H16, H14), 2.77 (s, 3H, $COCH_3$).

2.3. Instrumentation

^{1}H NMR (300 MHz) was measured on a Bruker Avance III 300

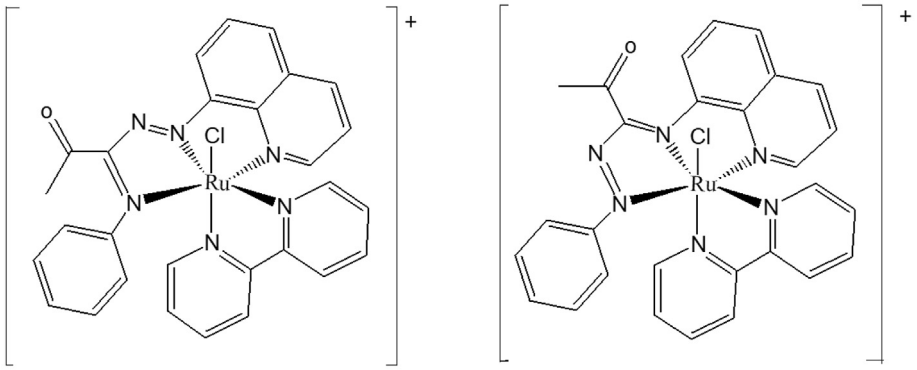

1 1A

Scheme 1. Structure of **1** and its published skeletal isomer **1A**.

spectrometer at room temperature. Elemental analyses were measured with a Eurovector E.A. 3000 instrument. IR spectra were collected on a Bruker Vertex FT-IR instrument. UV−Vis/NIR spectra were recorded on a Cary 5000 UV−Vis−NIR spectrometer. Catalytic activity was investigated using SCION 456-GC. Electrochemical measurements were performed in dichloromethane (Aldrich, HPLC grade) using Nova 2.11 workstation. Pt disk (2 mm) was thereby used as a working electrode with a Pt wire as a counter electrode and Ag wire as a pseudo-reference electrode. The temperature was controlled (at 25.0 ± 0.1 °C) by a Haake D8-G refrigerator. The ferrocene to ferrocenium oxidation was taken as internal reference [28,29]. UV/Vis and IR-spectroelectrochemistry of complex **1** were analyzed using an optically transparent thin layer electrochemistry (OTTLE) cell [30]. The potential was controlled by the Nova 2.11 workstation. At any given potential, the system allowed to reach equilibrium (i ~0 A) before the spectrum was taken.

2.4. Crystallography

A suitable crystal of complex **1** and its ligand H_2Y was mounted on a glass fiber and the data was collected using enhanced Mo radiation, $\lambda = 0.71073$ Å and Xcalibur/Oxford Diffractometer. CrysAlis Pro software was used for data collection, absorption correction and data reduction to give SHELX-format-*hkl* files [31]. The structure was solved using SHELXTL program package [32].

2.5. Computational methods

Full geometry optimization of 1 was carried out using density functional theory (DFT) at the B3LYP level [33]. All calculations were carried out using the GAUSSIAN 09 and Gauss-View program [34]. For C, H, Cl, N and O the cc-pvdz basis sets was assigned, while for Ru, the LanL2DZ basis set with effective core potential was employed [35]. Vertical electronic excitations based on B3LYP optimized geometries were computed using the time-dependent density functional theory (TD-DFT) formalism [36−38] in dichloromethane using conductor-like polarizable continuum model (CPCM) [36−38]. GaussSum was used to calculate the fractional contributions of various groups to each molecular orbital [39].

2.6. Catalytic hydrogenation of cinnamaldehyde

Complex **1** was tested as catalyst for the hydrogenation of cinnamaldehyde (mixture of 1:1 *cis*-to-trans) in a stainless-steel reactor (Parr-4842) equipped with a Waltow-945 unit to control the temperature of reaction and the stirring rate. In a typical experiment, the vessel was loaded with 0.040 g of Ru complex, (0.047 g) potassium hydroxide, (0.80 g) cinnamaldehyde and 100 mL 2-Propanol. The mixture was placed in the reactor and then tightly closed. The reactor temperature was adjusted to 86 °C before, hydrogen gas was added and adjusted to 4 bars. The course of the reactions was monitored by SCION 456-GC. various time intervals (SCION, FID, 30-m crosslinked FAFF capillary column).

3. Results and discussion

3.1. Synthesis

The new quinoline−azoimine ligand (H_2Y= C_6H_5NH-$C(COCH_3)$ = N-NHC_9H_6N) was prepared by reacting ((1Z)-2-oxo-N-quinoline-8-ylpropanehydrazonoyl chloride, aniline and triethylamine in refluxing ethanol (Scheme 2).

Pure H_2Y was obtained by recrystallization from ethanol. The structure of H_2Y was confirmed by elemental analysis, ^{1}H NMR spectroscopy and X-ray diffraction. The ATR spectrum of H_2Y showed intense absorption bands at 3240 cm^{-1}, 1688 cm^{-1} and 1570 cm^{-1} which are assigned to the stretching frequencies of the two NH groups, C=O of the acetyl group, and the C=N group, respectively. In addition to the phenyl protons, the ^{1}H NMR spectrum of H_2Y showed a sharp singlet at 2.6 ppm assigned for the acetyl H_3CCO group. The two resolved singlet signals at $\delta = 9.03$ ppm and at $\delta = 7.44$ ppm with integral ratio of 1:1 are assigned to the two NH groups. In contrast to the NMR results, the solid ATR spectrum of H_2Y showed only one characteristic, intense absorption band for the two NH groups. It seems that the two NH stretching frequencies are very close in energy and cannot be discriminated and resolved in the solid-state ATR, most presumably because of the broadening of the NH bands. There is only one structural isomer for H_2Y ligand which is confirmed by the presence of only one signal for each hydrogen in the ^{1}H NMR spectrum.

$[Ru^{II}(Y)(bpy)Cl](ClO_4)$ (**1**) was prepared according to a previously published procedure [19] by the stepwise addition of equimolar amounts of H_2Y, $RuCl_3$ and bpy into boiling ethanol. The counter ion PF_6^- was here replaced by ClO_4^- to get a good-quality single crystal suitable for x-ray diffraction analysis (Scheme 1). The coordination sphere around the ruthenium ion consists of a chloride ligand, three nitrogens from Y (azo-N, imine-N′ and quinolone-N″) and two bpy nitrogen donor atoms. During the reaction, ruthenium(III) has undergone a one-electron reduction and the ligand H_2Y is oxidized to azoimine (Y). Also, ethanol presumably acts both as a solvent and as a reducing agent for Ru(III). No N-H bands is observed in the IR spectrum for complex **1** confirming the loss of the two dissociable protons of the NH groups. The complex **1** has a sharp absorption bands at 1667 cm^{-1}, 1606 cm^{-1} and 1505 cm^{-1} which are assigned to stretching frequencies for the C=O, C=N, and N=N groups, respectively. In the ^{1}H NMR spectrum, the two signals corresponding to NH group of the azoimine are also absent supporting the full oxidation to azoimine moiety. The aromatic region of H_2Y and **1** showed several resonance multiplets due to the aromatic protons of the phenyl rings of H_2Y and bpy ligands.

3.2. Crystal structures

Crystal structure data and selected bond lengths and angles for the ligand H_2Y as well as $[Ru(Y)(bpy)Cl](ClO_4)$ (**1**) are presented in Table 1 and Table 2, respectively. ORTEP drawing of complex **1** and H_2Y are shown in Fig. 1 and Fig. 2, respectively. H_2Y crystallized in the triclinic system while complex **1** crystallized in the monoclinic space group P $2_1/c$. The bond length for N(12)-N(11) is 1.343(2) Å in H_2Y. The bond length for N(12)-C(13) is 1.295(2) Å which is shorter than N(16)-C(13) (1.386(2)Å). The azo group is coplanar with the quinoline ring, the deviation of N11 and N12 atoms from the mean plane of the quinoline ring is 0.10 Å and 0.29 Å, it is stabilized by the intramolecular N11-H···N1 hydrogen bonding interactions. The parameters of this interactions are 2.67 Å, 2.33 Å and 103.9°. This planarity is reinforced by the extended delocalization of the π-system of the quinoline ring to include the azo group. The N(12)-N(11) and C(10)-N(11) bond lengths are 1.343 Å and 1.387 Å, respectively, which are shorter than the corresponding single bonds and longer the corresponding double bonds. The N16-H···O5 hydrogen bond interactions connect the molecular units of the ligand to form dimer structure (Fig. S1, top), the hydrogen bonding interaction parameters are 2.96 Å, 2.19 Å and 148.6°, respectively. C-H···N(π) interactions connect the dimers to form a layer structure in the bc crystallographic plane (Fig. S1, bottom). The parameters of these interactions are listed in Table 3. For Complex **1**, The ligand H_2Y is coordinated to ruthenium as a tridentate N, N′, N″-donor and in meridional fashion; the bpy ligand is in *cis* orientation.

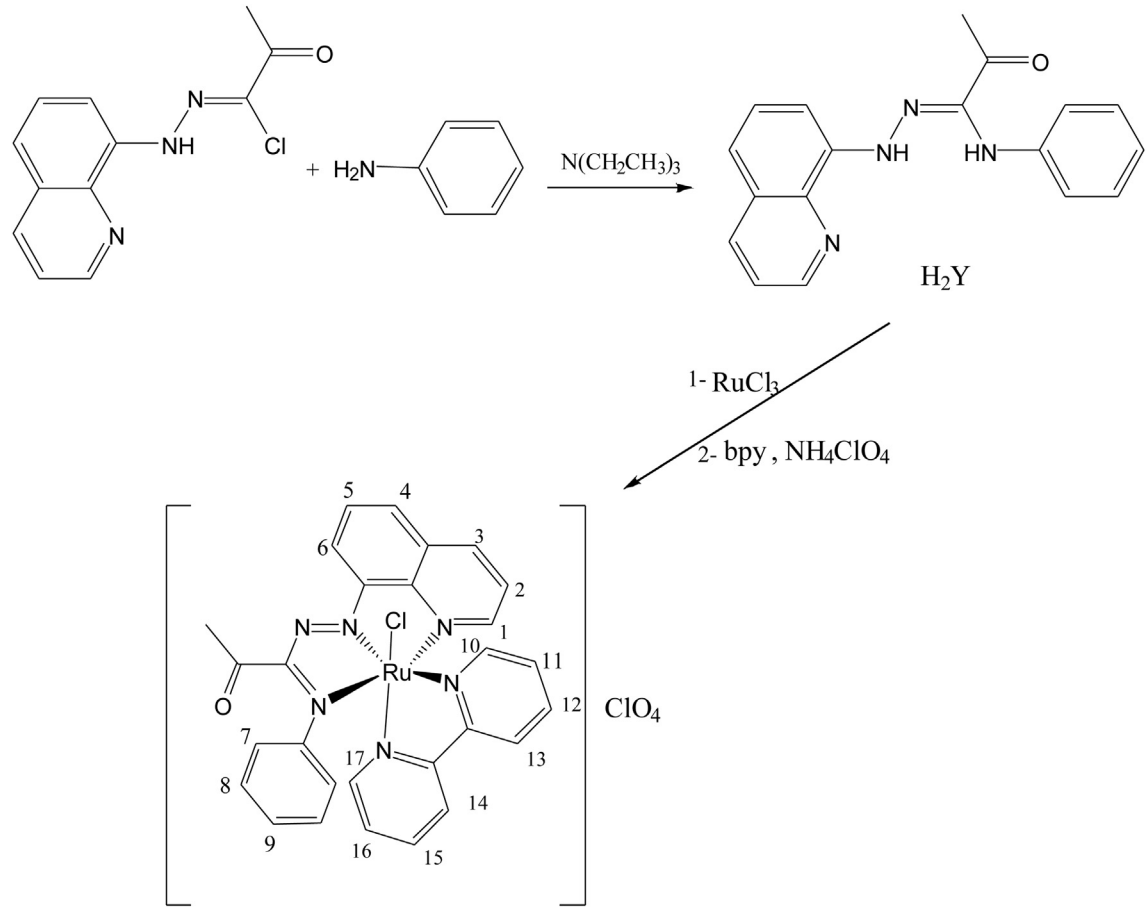

Scheme 2. Synthesis of [Ru(Y)(bpy)Cl](ClO$_4$).

Table 1
Crystal data and structure refinement for Ligand (H_2Y) and complex **1**.

	Ligand H_2Y	Complex 1
Empirical formula	$C_{18}H_{16}N_4O$	C_{29} H_{24} Cl_4 N_6 O_5 Ru
Formula weight	304.35	779.41
Temperature	293(2) K	293(2) K
Wavelength	0.71073 Å	0.71073 Å
Crystal system	Triclinic	Monoclinic
Space group	P −1	P 21/c
Unit cell dimensions	a = 7.3903(6) Å, α = 105.595(8)°α = 105.595(8)°. b = 10.3828(9)Å, β = 99.047(8)° c = 11.2688(11) Å, γ = 100.194(7).	a = 8.2795 Å, α = 90 b = 32.318(2) Å, β = 96.263(6)°. c = 12.0898(10) Å, γ = 90°.
Volume	800.34(12) Å^3	2591.8(2) Å^3
Z	2	4
Density (calculated)	1.263 Mg/m^3	1.610 Mg/m^3
Absorption coefficient	0.082 mm^{-1}	0.868 mm^{-1}
F(000)	320	1568
Crystal size	0.42 × 0.32 × 0.25 mm^3	0.4220 × 0.3315 × 0.1377 mm^3
Theta range for data collection	3.14–25.00°..	2.91–25.00°
Index ranges	−7 ≤ h ≤ 8, −12 ≤ k ≤ 12, −13 ≤ l ≤ 13	−9 ≤ h ≤ 9, −38 ≤ k ≤ 28, −14≤ l ≤ 14
Reflections collected	5727	17111
Independent reflections	2820 [R(int) = 0.0215]	5659 [R(int) = 0.0423]
Completeness to theta = 26.30°	99.8%	99.8%
Absorption correction	Semi-empirical from equivalents	Semi-empirical from equivalents
Max. and min. transmission	1.00000 and 0.91278	1.00000 and 0.62877
Refinement method	Full-matrix least-squares on F^2	Full-matrix least-squares on F^2
Data/restraints/parameters	2820/0/208	5659/0/406
Goodness-of-fit on F^2	1.040	1.203
Final R indices [I > 2sigma(I)]	R1 = 0.0526, w$R2$ = 0.1217	R1 = 0.0788, w$R2$ = 0.1616
R indices (all data)	R1 = 0.0820, w$R2$ = 0.1485	R1 = 0.0997, w$R2$ = 0.1712
Largest diff. peak and hole	0.216 and −0.181 eÅ^{-3}	0.586 and −0.696 e.Å^{-3}

$R_1 = \Sigma||F_o| - |F_c||/\Sigma|F_o|$; $wR_2 = \{\Sigma[\ w(F_o^2 - F_c^2)^2]/\Sigma\ [w(F_o^2)^2]\}^{1/2}$.

Table 2
Selected bond lengths and angles for complex **1**, and its oxidized (**1**+) as well as reduced (**1-**) forms.

H_2Y		Complex			
		1		1^-	1^+
Bond lengths (Å) (experimental)		Bond lengths (Å)(experimental, calculated)		Bond lengths (Å)(calculated)	
N(12)-N(11)	1.343(2)	Ru(1)-N(11)	1.889(6), 1.932	1.972	1.972
N(16)-C(13)	1.386(2)	Ru(1)-N(16)	2.008(5), 2.056	2.079	2.090
N(12)-C(13)	1.295(2)	Ru(1)-N(34)	2.068(6), 2.118	2.089	2.127
O(5)-C(14)	1.220(2)	Ru(1)-N(1)	2.084(5), 2.157	2.155	2.141
C(13)-C(14)	1.476(3)	Ru(1)-N(23)	2.117(6), 2.180	2.145	2.172
		Ru(1)-Cl(2)	2.3559(19), 2.402	2.448	2.337
		N(11)-N(12)	1.322(7), 1.297	1.331	1.289
		N(16)-C(13)	1.319(9), 1.328	1.351	1.332
Bond angles (°)		Bond angles (°) (experimental, calculated)		Bond angles (°) (calculated)	
C(13)-N(12)-N(11)	118.67(16)	N(11)-Ru(1)-N(16)	77.8(2), 76.7	76.7	75.9
C(13)-N(16)-C(17)	124.91(17)	N(11)-Ru(1)-N(34)	98.2(2), 101.0	98.1	101.9
N(12)-N(11)-C(10)	119.26(16)	N(16)-Ru(1)-N(34)	89.4(2), 93.8	92.6	86.8
N(12)-N(11)-H(11A)	120.4	N(11)-Ru(1)-N(1)	81.9(2), 80.9	79.7	79.9
O(5)-C(14)-C(15)	121.40(18)	N(16)-Ru(1)-N(1)	159.4(2), 157.6	156.4	154.3
O(5)-C(14)-C(13	119.48(18)	N(1)-Ru(1)- N(34)	90.3(2), 90.9	92.5	90.0
N(12)-C(13)-C(14)	115.65(17)	N(11)-Ru(1)-N(23)	175.2(2), 176.4	174.9	177.3
N(16)-C(13)-C(14)	117.77(17)	N(16)-Ru(1)-N(23)	99.5(2), 101.3	101.6	106.1
N(12)-N(11)-C(10)	119.26(16)	N(34)-Ru(1)-N(23)	77.7(3), 76.0	77.0	76.5
N(12)-C(13)-N(16)	126.50(18)	N(1)-Ru(1)-N(23)	100.5(2), 101.1	102.0	97.8

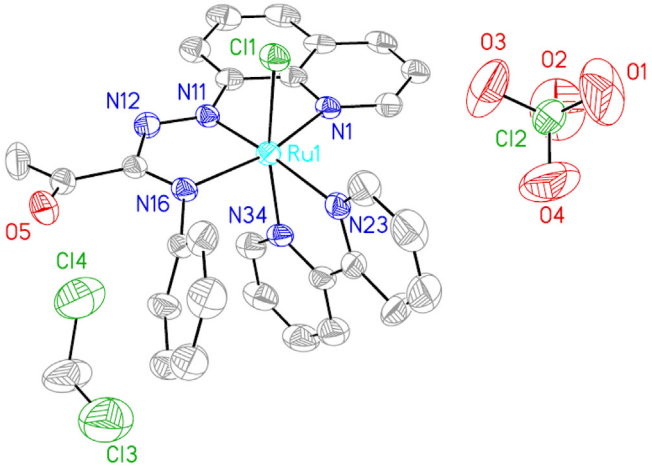

Fig. 1. ORTEP of complex 1. Thermal ellipsoids of ORTEP plots are reported at 30% probability.

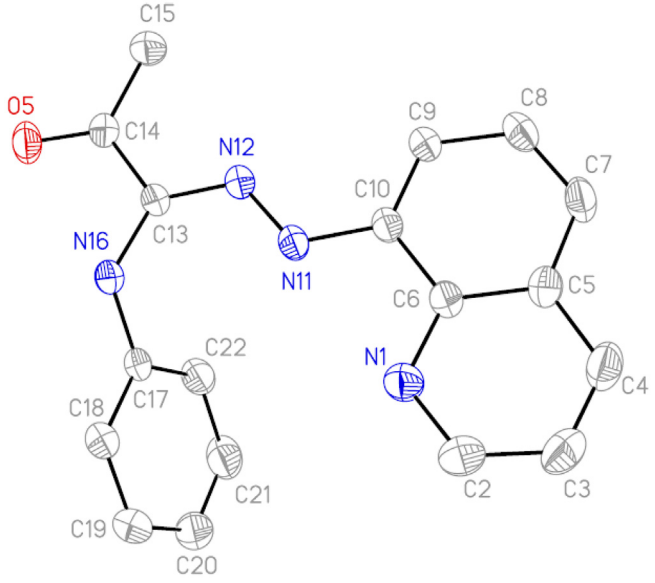

Fig. 2. ORTEP of ligand (H2Y). Thermal ellipsoids of ORTEP plots are reported at 30% probability.

Table 3
C-H···N(π) interaction distances (Å) and angles (°) in the ligand (H_2Y).

Interaction	C21-H···N1(π)	C15-H···N1(π)
C···N	3.498	3.787
H···N	2.694	2.867
C-H···N	145.3	160.7

The average bond length for Ru—N(bpy) is 2.093 Å. The azomethine ligand is known to interact strongly with the Ru(II) center via the dπ—π* interactions [24–27]. This has been reflected in the average Ru(1)-N(11) (Azo) bond length (1.889(6)Å) and the Ru(1)-N(16)(methine) bond length (2.008(5)Å). The shortening in the bond length for Ru—azoimine fragment compared to that of Ru—N(1)(pyridine) (2.093 Å) indicates that the M—L π interaction is localized in the M—Azo fragment [19,24–27]. The bond angles in the five membered ring described by the coordination of an azoimine (N(11)-Ru(1)-N(16)), iminepyridine N(11)-Ru(1)-N(1) and bpy N(34)-Ru(1)-N(23) are 77.8(2)°, 81.9(2) ° and 77.7(3) °, respectively.

The supramolecularity of the complex is mainly developed based on the non-classical C-H…A hydrogen bonding interactions (A = O or Cl) and C=O···C π interactions. The parameters of the hydrogen bonding interactions are listed in Table 4. Furthermore, C4-H···Cl1 hydrogen bonding and C=O···C π interactions connect the cationic complex molecules to form a chain structure parallel to the a-axis (Fig. S2, top). The C=O…Cπ interaction lengths are 2.99 Å, 4.02 Å and 142.4° for C33···O5, C14···O5 and C14 = O5···C33, respectively. Subsequently, the C-H…A hydrogen bonding interactions link the ClO_4^- anion, dichloromethane and the cationic molecules of the complex to form the final three-dimensional structure (Fig. S2, bottom).

For **1**, the difference between the (Ru-N11 and Ru-N16) bond distances is significant (0.12 Å). Whereas, the average of (Ru-N11 and Ru-N16) is 1.949 Å which is equal, within the experimental

Table 4
C-H…A Interactions distances (Å) and angles (°) in the ligand (H_2Y) where A = Cl or O.

C-H…A	C…A	H…A	C-H…A
C4-H···Cl1	3.58	2.78	144.1
C2-H···O3	3.36	2.67	131.5
C31-H···O1	3.19	2.48	133.0
C15-H···Cl4	3.72	2.94	138.6
C1-H···O2	3.55	2.68	148.6

Table 5
Ru—N and N=N bond distances (Å) for **1** and **1A**.

Complex	1		1A	
	Optimized	Experimental	Optimized	Experimental
Ru—N(azo)	1.932	1.889	2.035	1.945
Ru—N(imine)	2.055	2.008	2.008	1.960
N=N	1.297	1.322	1.299	1.313

error, to the corresponding value (1.953 Å) in its skeletal isomer [Ru(L1)(bpy)Cl](PF_6) (**1A**)(Scheme 1). However, it is interesting to note that the bond lengths Ru—N(Azo ((1.889(6) (Å) for complex **1** are significantly shorter than the corresponding lengths of its reported skeletal isomer **1A** (Ru—N(azo) = 1.945 (3) Å and N=N bond distance (1.322(7) Å) in is longer than the corresponding distance in 1A (1.313(4) Å) [19]). Aslo the Ru-N(azo) bond distances is shorter than the Ru-N(imine) in the two complexes (Table F1). However, the difference in the bond distances is quite large in 1 is 0.12 Å whereas it is significantly small in 1A (0.02 Å. Theoretical calculations were used to rationalize the differences in bond distances in the coordination sphere in complex (**1**) and (**1A**). The two complex-cations were optimized using the crystal structure coordinate as starting geometry. The difference between the optimized (Ru-N11 and Ru-N16(imine) bond distances is 0.12 Å, whereas the corresponding value in 1A is 0.03 Å, which agrees with the values obtained from the crystal structures (Table 5). The percent distribution of the frontier orbitals in the cationic complexes was carried out using GaussSum program [39] (Table 6, Fig. 3). A closer look at the LUMO orbitals of the two cationic complexes shows two interesting observations; (a) For both complexes the LUMO is constructed from the azoimine—quinoline (L and Y) Ligand while the for the HOMOs, the first three highest energy orbitals are Ru in character. The significant contribution from Ru(II) to the LUMO can be correlated to the significant π-back donation from the metal d orbital to azoimine-qinoline ligands (Table 6, Fig. 3) [40]. (b) in the two complexes, not any part of the LUMO is located on the bipyridine ligand c) The LUMO is mainly azo in character, but in **1A** it is extended over the quinoline which is trans to the azo group. The shortening in the Ru(II)- azo bond in **1A** relative to that in **1** can be rationalized by the amount of the back donation or MLCT from Ru(II) to the azo group and by the *trans*-effect, as well. The atom

Table 6
DFT energies and % composition of selected molecular orbitals (LUMO (L) and HOMO (H)) for **1** and its published skeletal isomer **1A** [19] expressed in terms of composing fragments.

M.O	eV		Ru		Azo		Ph		8-Aminoqu.		bpy		Cl	
	1	1A	1	1A	1	1A	1	1A	1	1A	1	1A	1	1A
L +3	−4.48	−4.46	2	2	0	1	0	0	2	1	96	95	0	0
L +2	−5.03	−4.83	2	2	18	10	1	2	79	86	0	1	0	0
L +1	−5.29	−5.32	4	4	0	0	0	0	0	1	95	95	0	0
L	−6.21	−6.15	23	21	47	49	3	12	22	14	2	1	3	3
H	−8.48	−8.4	36	48	15	9	22	1	7	12	2	4	17	25
H-1	−8.7	−8.77	30	36	16	10	34	8	3	3	4	3	12	40
H-2	−8.96	−9.11	30	38	14	10	1	11	5	20	3	6	47	15
H-3	−9.23	−9.18	5	38	3	12	90	10	0	23	1	5	0	12

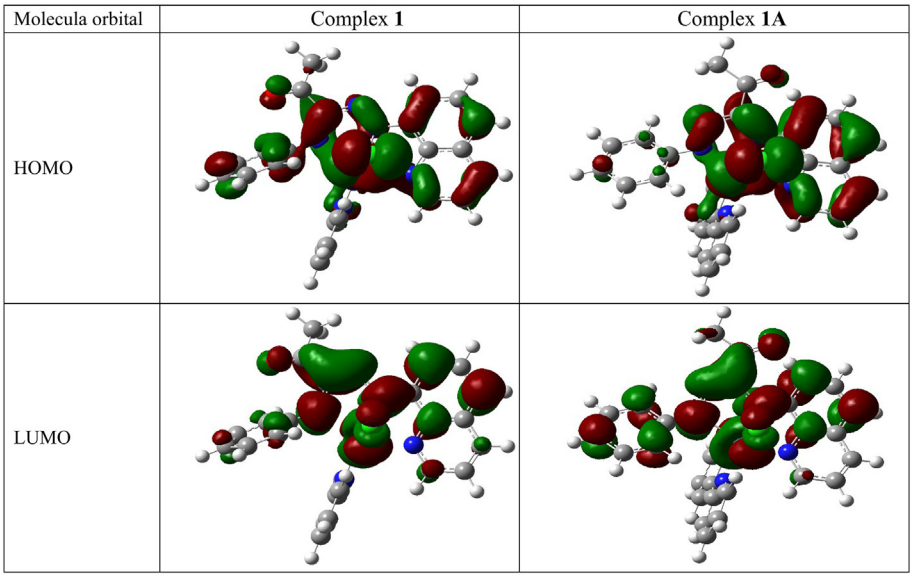

Fig. 3. Isodensity plot for HOMOs and LUMOs of Complex 1 and complex 1A.

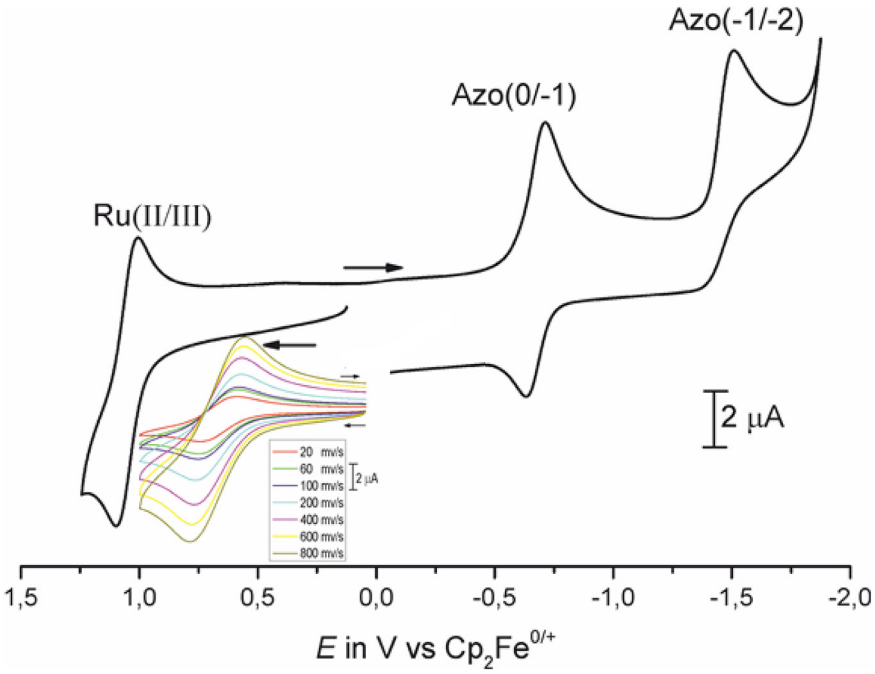

Fig. 4. Cyclic voltammogram of complex 1 vs. Cp2Fe0/+ (TBAHF, 0.1 M, dichloromethane, 25 °C). Inset shows the Ru(II/III) couple at different scan rates.

trans to the azo group in **1** is the bipyridyl nitrogen N23 (Fig. 3), while, it is the quinoline nitrogen in **1A**. So the shortening of Ru-N11(Azo) (1.889(6) Å) and the elongation of Ru-N34(azo) (2.117(6) Å) in **1A** can be explained as follows: In IA, there is some back donation from Ru(II) to the *trans*-quinoline which reduces the back donation to the azo group, while in 1, the azo is trans to bpy and so the back donation is localized in the Ru(II)-azo bond [40].

3.3. Electrochemistry

The cyclic voltammogram for complex 1 is shown in Fig. 4. Inset Fig. 4 shows the oxidation peak (1.05 V) at different scan rates, the small change of peak potentials with scan rates meaning that the it is quasi-reversible oxidation process. Since the HOMO of 1 has a metal contribution of about 36%, the couple at 1.05 V has been assigned to Ru(III/II). On the other hand, the ligand azo moiety contributes by about of 47% to the LUMO; thus the reduction couples at −1.15 and −1.75 V vs. $Cp_2Fe^{0/+}$ (cathodic wave peak maxima) can be assigned to L(0/-) and L(−/−2). The anodic shift for Ru(III/II) and the cathodic shift for L(0/-) in [Ru(Y)(bpy)Cl](ClO_4) (**1**) compared to that in [Ru(L1)(bpy)Cl](PF_6) (**1A**) (Ru (III/II) = 0.98 V and L(0/-) = −1.30 V) suggests that the ligand Y is a better π-acceptor ligand compared to the previously prepared azomine bidentate ligand L1 [19].

3.4. Electronic structure and DFT calculations

The electronic absorption spectrum of complex (**1**) was measured using acetonitrile as a solvent (Fig. 5). The complex exhibits an intense transition in the UV region (220–320 nm) accompanied by a moderately intense band at longer wavelength (320–550 nm). To assign these bands, TD-DFT calculations on the optimized geometries of **1** was performed using GAUSSIAN 09 program [34]. The calculated bond lengths and angles are reproduced well in agreement with the X-ray determined structure (Table 2). Relative percentages of atomic contributions to the lowest unoccupied and highest occupied molecular orbitals have been placed in Table 7. Moreover, the isodensity plots for the HOMOs and LUMOs orbitals are shown in Fig. 3. DFT results of **1** show that the HOMO to HOMO-3 are mainly Ru and azoimine (Y) in character. The LUMO, LUMO+2 and LUMO+3 molecular orbital are mainly azoimine in a character. The LUMO has 24% metal d orbital Ru character suggesting significant back donation (Table 4) [40].

Computation of 30 excited states of complex **1** allowed the interpretation of the experimental spectra for the complexes in the 300–800 nm range (Table 8). The theoretical absorption spectrum was simulated using GaussSum software [39]. Both the experimental UV–Vis spectrum of complex **1** reported in acetonitrile and its simulated absorption spectrum (inset Fig. 5) were in acceptable agreement. The intense absorption band at 300 (350 calculated) is results mainly from HOMO-10 (Y in character)→LUMO (Y in character) (44%), thus this band is assigned as ligand-to-ligand charge transfer LLCT (Y(π))→Y(π*)) (Table 8). The band centered at 370 (374 calculated) results from HOMO-1 (mainly Ru and bpy) →L+1(bpy in character) (49%), thus this band is assigned to metal–ligand-to-ligand charge transfer (Ru(dπ), L(bpy))→ bpy (π*)) MLLCT [41–43]. The band centered at 410 (411 nm calculated) results from HOMO (Ru and Y in character) →L+2 (bpy in character) (72%) thus this band is assigned as metal–ligand-to-ligand charge transfer (Ru(dπ), Y(π))→bpy(π*)) MLLCT. The band centered at 500 (527 calculated) results from HOMO-2→LUMO (69%) thus this band is assigned as metal-Ligand charge transfer (Ru(dπ)→Y(π*)) MLCT.

UV/Vis spectroelectrochemical measurements were performed on complex **1** in acetonitrile in order to obtain the electronic absorption spectra for **1**+ (Fig. 6). Upon oxidation there is a complete disappearance of the MLLCT bands at 374 and 430 nm and the appearance of a new band near 650 nm. The oxidation of **1** is reversible with greater than 95% recovery of the Ru-(II) complex spectrum.

Theoretical calculations were performed on the oxidized form (**1**+); the calculations utilize both α and β occupied molecular orbitals. Relative percentages of atomic contributions to the lowest

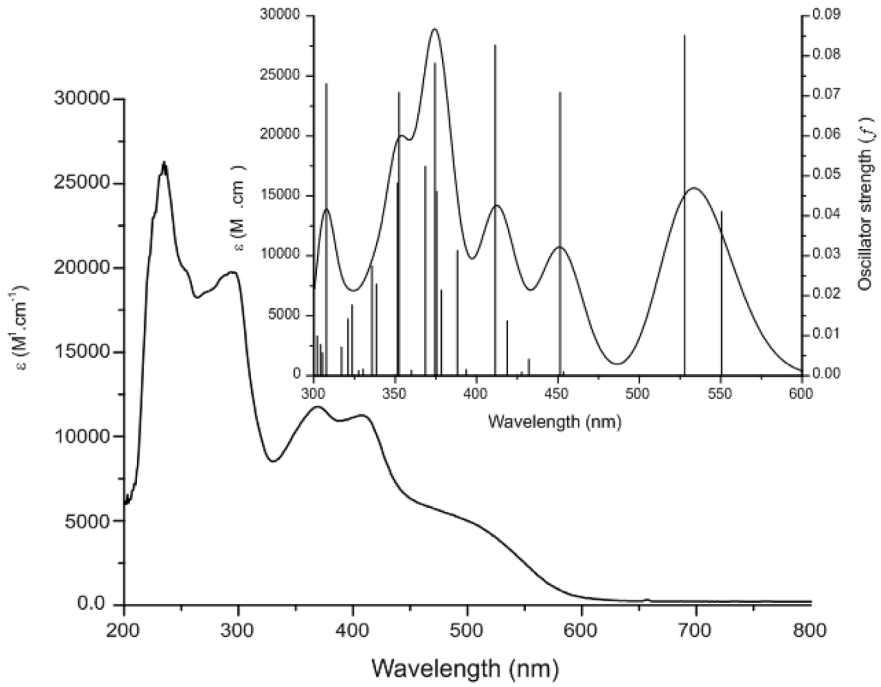

Fig. 5. UV–Vis of complex 1 in CH3CN. Inset shows simulated absorption spectrum of complex 1. (Black line) based on TD-DFT calculations, compared to excitation energies and oscillator strengths.

Table 7
Relative Percentages of Atomic Contributions to the Lowest Unoccupied and Highest Occupied Molecular Orbitals (LUMO (L) and HOMO (H)) of **1** in acetonitrile.

Complex		eV	Ru	Cl	Azo	bpy
1	L+5	−1.49	3	0	2	95
	L+4	−1.75	5	0	26	69
	L+3	−1.8	3	0	72	24
	L+2	−2.61	1	0	82	16
	L+1	−2.64	3	0	17	80
	L	−3.93	24	2	73	1
	H	−6.28	50	13	33	3
	H-1	−6.6	44	3	46	7
	H-2	−6.84	42	32	23	3
	H-3	−7.08	34	6	53	7
	H-4	−7.3	1	0	96	3
	H-5	−7.36	6	22	61	11

unoccupied and highest occupied molecular orbitals have been placed in Table S1. Moreover, the isodensity plots for the HOMOs and LUMOs orbitals are shown in Fig. S3. Ru(III) does significantly contribute to LUMO of β-spin and HOMO-2, HOMO-4 of α-spin and β-spin. HOMO to HOMO-3 of α-spin and β-spin and LUMO to LUMO +1 of α spin and (LUMO, LUMO+2) are mainly azoimine (Y) in character. Chloride mainly contributes to HOMO-2 of β-spin and HOMO-3 of α-spin.

The theoretical absorption spectrum for (**1**+) was simulated using GaussSum software [39] (inset Fig. 6, Table 8). The intense absorption band at 650 nm (689 calculated) results mainly from HOMO(β) and HOMO (α) which are (Y in character)→LUMO+1(β) and LUMO(α) (Y in character) thus this band is assigned as ligand-to-ligand charge transfer (Y(π)→Y(π*)). The band centered at 550 nm (602 nm calculated) results from HOMO-2(α) (Ru and

Table 8
Computed excitation energies (nm), electronic transition configurations and oscillator strengths (f) for the optical transitions of complex **1**, and its oxidized (**1**+) as well as reduced (**1-**) forms.

Complex	λ (nm)	Osc. Str.	Major contribs
1	528	0.085	H-3→L (23%), H-2→L (74%)
	451	0.071	H-5→L (87%)
	412	0.083	H→L+2 (72%), H→L+6 (13%)
	374	0.078	H-1→L+1 (53%), H-1→L+2 (30%)
	369	0.052	H-9→L (55%), H-8→L (27%)
	352	0.071	H-10→L (44%), H-1→L+6 (14%), H→L+3 (16%)
1-	1094	0.010	H (β) →L (β) (98%)
	769	0.050	H (A) →L+1(A) (90%)
	674	0.041	H-2(β) →L (β) (70%), H-1(β) →L (β) (28%)
	494	0.057	H (α) →L+3(A) (16%), H-3(β) →L (β) (64%)
	470	0.124	H-1(α) →L+1(α) (53%), H (β) →L+2(β) (29%)
	447	0.055	H-2(α) →L (α) (44%), H-4(β) →L (β) (23%), H-1(β) →L+1(β) (19%)
	442	0.048	H-2(α) →L (α) (12%), H (α) →L+5(α) (52%)
1+	689	0.100	H (α) →L (α) (18%), H (β) →L+1(β) (39%)
	602	0.045	H-2(α) →L (α) (20%), H-5(β) →L+1(β) (26%), H-4(β) →L+1(β) (14%)
	483	0.055	H-5(α) →L (α) (13%), H-12(β) →L (β) (16%), H-9(β) →L (β) (23%)
	472	0.155	H-9(β) →L (β) (16%), H-8(β) →L (β) (11%), H-6(β) →L+1 β) (19%), H-5(β) →L+1(β) (14%)

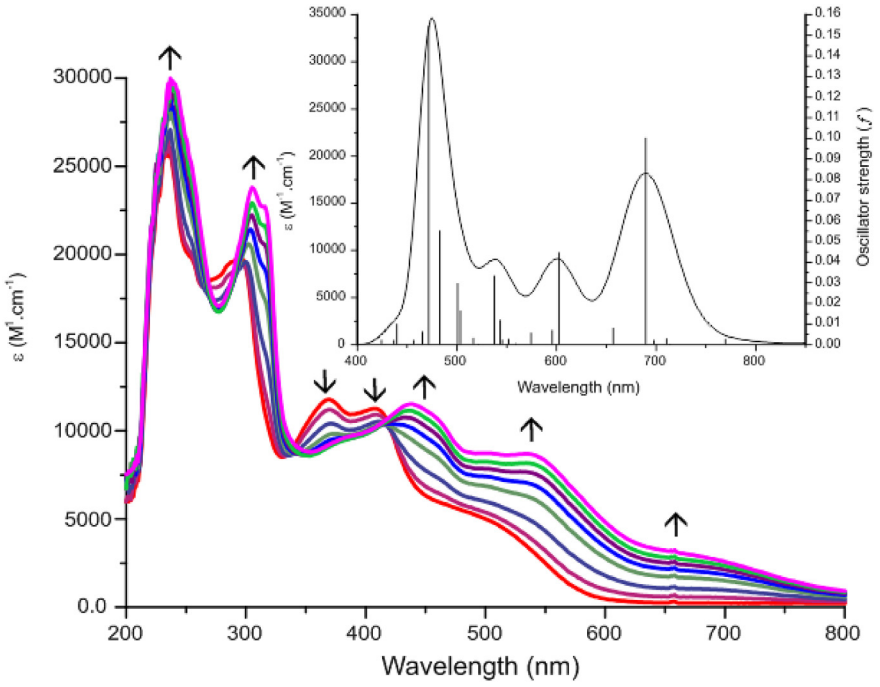

Fig. 6. UV−Vis Spectroscopic changes on oxidation of complex 1 (CH3CN/NBu4PF6, r.t.). . Inset shows simulated absorption spectrum of complex 1+. (Black line) based on TD-DFT calculations, compared to excitation energies and oscillator strengths.

azoimine character)→LUMO(α) (Y in character), HOMO-5(β) (bpy in character) and HOMO-4(β) (Ru in character)→LUMO+1(β) (Y in character) thus this band is assigned as (Ru(dπ), Y(π))→bpy(π*)) MLLCT [41–43]. The band centered at 450 nm (471 nm calculated) results from HOMO-8 (β) (Chloride in character)→LUMO(β) (Ru in character) thus this band is assigned to Ligand Metal Charge Transfer (LMCT).

UV/Vis spectroelectrochemistry (Fig. 7) on the reduced species **1-** was performed in acetonitrile in order to reduce Ru(II) to Ru(I). Theoretical calculations were performed to assign the experimental bands. Relative percentages of atomic contributions to the lowest unoccupied and highest occupied molecular orbitals have been placed in Table S1. Moreover, the isodensity plots for the HOMOs and LUMOs orbitals are shown in Fig. S3. For α and β spin, HOMO to HOMO-3 are mainly Ru in character with a significant contribution of azoimine ligand (Y). While β-spin of LUMO+1 and LUMO+3 is mainly bpy, α-spin is azoimine in character. Also, while α-spin of LUMO and LUMO+2 is mainly bpy in character β-spin is mainly

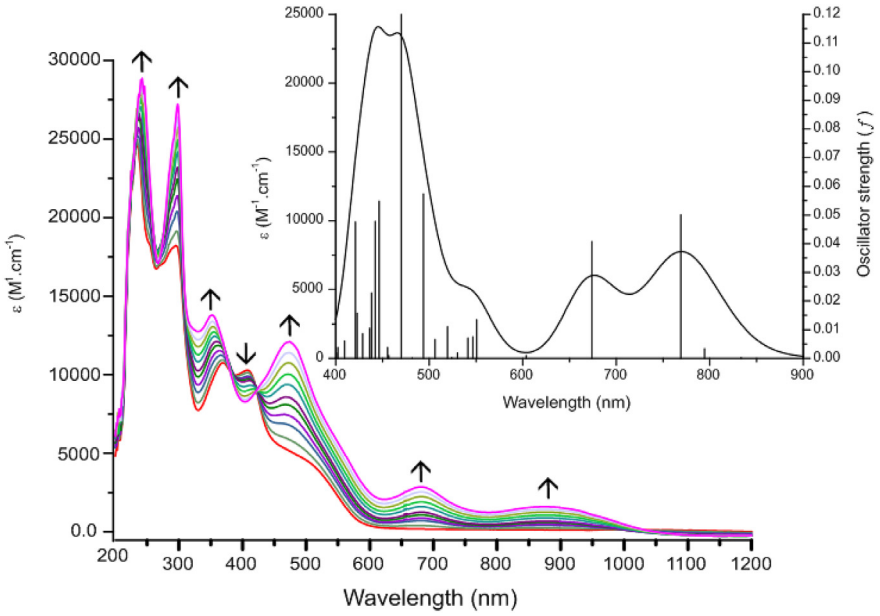

Fig. 7. UV/Vis/near-IR Spectroscopic changes on Reduction of complex 1 (CH3CN/NBu4PF6, r.t.). Inset shows simulated absorption spectrum of complex 1-. (Black line) based on TD-DFT calculations, compared to excitation energies and oscillator strengths.

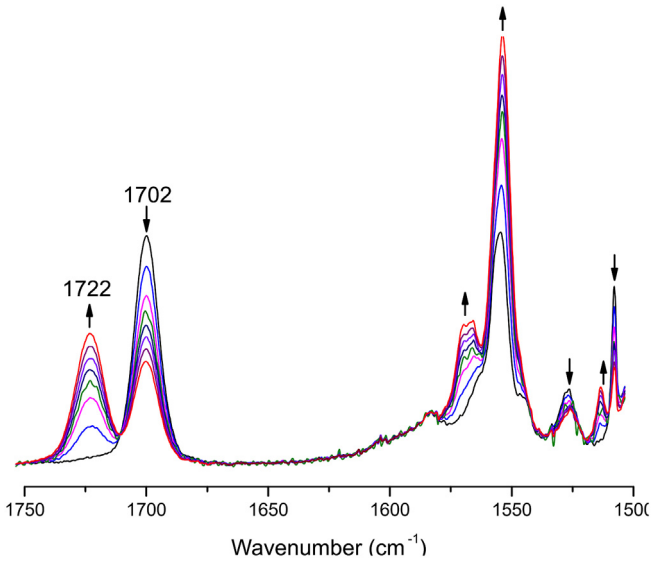

Fig. 8. IR spectroscopic changes upon the oxidation of complex 1 (CH2Cl2/NBu4PF6).

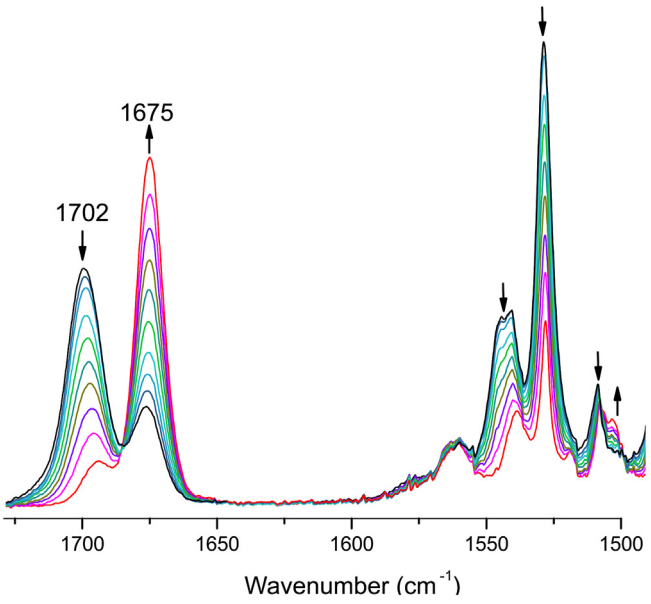

Fig. 9. IR spectroscopic changes upon the full reduction of complex 1 CH2Cl2/NBu4PF6).

azoimine in character.

TDDFT calculation was used to interpret the electronic spectrum of the reduced species **1-** (inset Fig. 7, Table 8). The band centered at 900 nm (1093 nm calculated) results from HOMO(β) (mainly of Ru(I)) →LUMO(β) (Y in character), thus this band is assigned as (Ru(dπ))→bpy(π*)) (MLCT). The band centered at 675 nm (674 calculated) results from HOMO(α) (Y and Ru(I) in character) →LUMO+1(α) (Y in character), thus this band is assigned as (Ru(dπ), Y(π))→Y(π*)) (MLLCT). The band centered at 465 nm (470 calculated) results from HOMO-1(α) and HOMO(β) (Ru(I) in character)→ LUMO+1(α) and LUMO+2(β) (Y in character) thus this band is assigned as MLCT **.**

3.5. Infrared spectroelectrochemistry

IR spectroelectrochemistry is a powerful tool to estimate the degree of charge delocalization between metal and π-acidic ligand upon oxidation/reduction processes. Fig. 8 and Fig. 9 show the IR changes of complex 1 during the oxidation and reduction process, respectively. The oxidation (Fig. 8) is reversible; however, the reduction (Fig. 9) has a poor reversibility. Figs. 8 and 9 show the IR spectrum of complex **1**+ in dichloromethane (black line). The complex shows intense vibrational bands at 1702 cm^{-1}, 1606 cm^{-1} and 1590 cm^{-1} which are assigned to the C=O, C=N, and N=N stretches, respectively. Upon oxidation of complex **1** to **1**+ (Fig. 8), the C=O band is successively blue-shifted from 1702 cm^{-1} to 1726 cm^{-1}. This blue shift for C=O, which is conjugated with the azo and imine moiety, is due to a decrease in back donation to π* of non-innocent azoimine moiety upon oxidation. On the other hand, there is only a slight shift with increasing intensity of the C=N and N=N bonds. The reduction of the complex **1** to **1-** (Fig. 9) showed an increase in intensity and a slight red shift in energy for the C=O bond from 1702 cm^{-1} to 1675 cm^{-1}. The red shift can be explained by the reduction of the azo group which is conjugated to the C=O supported by the cyclic voltammetry and non-innocent behavior of this ligand.

3.6. Hydrogenation of cinnamaldhyde (CALD)

Cinnamaldehyde has been selected as a model substrate for hydrogenation under mild condition. Scheme 3 shows the different regio-selective hydrogenation possibilities of cinnamaldehyde.

In the hydrogenation of ketones and aldehydes homogeneously catalyzed by Ru complexes the active catalyst form is believed to be a hydride/dihydride Ru complex that forms under reaction conditions [44]. The actual catalyst must thus be prepared before a conversion of cinnamaldehyde is observed, which explains the induction period in Fig. 10 at the begin of reaction. Although the molar Ru: CALD ratio is relatively high (1: 68), complex **1** shows only a rather low activity and moderate selectivity (Fig. 10). It took 14 h of reaction under indicated conditions for a conversion to approach 70%. The percentage of cinnamyl alcohol (the desired component) is thereby only 26% corresponding to a reaction selectivity to cinnamyl alcohol of 37%. Maximum concentration of hydrocinnamaldehyde (saturated aldehyde), which forms undesirably in a parallel route, is reached in 9 h of reaction (HCALD % = 18%) but decreases thereafter due to consecutive hydrogenation to phenylpropanol (PP). In a previous study, a related Ru(II) complex, namely [Ru(PhN = NC($COCH_3$) = NPhSPh)(bpy)Cl_2], was reported to show a much higher activity in the hydrogenation of cinnamaldehyde under similar conditions, reaching more than 90% conversion in 4 h with a cinnamyl alcohol selectivity exceeding 90% [45].

4. Conclusion

A new octahedral ruthenium(II) complex having the general formula [Ru^{II}(Y)(bpy)Cl](ClO_4) {Y= C_6H_5N=C($COCH_3$)N=NC_9H_6N and bpy = 2,2′-bipyrdine} (**1**) was synthesized. The bonding in **1** and its published skeletal isomer [Ru^{II}(L1)(bpy)Cl](PF_6) {L1 = C_6H_5N=N-($COCH_3$)C=NC_9H_6N} (**1A**) has been analyzed using molecular orbital theory. Complex **1** is stabilized by the strong π-acceptor quinoline−azoimine ligand H_2Y and showing the Ru(III/II) couple at 1.05 V vs. Cp_2Fe/Cp_2Fe^+. The UV/Vis and IR spectra for **1, 1+, 1-** was investigated by spectroelctrochemistry and their electronic bands and electronic structures was interpreted using DFT and TDDFT calculations. Complex **1** has a moderate activity for the hydrogenation of α, β-unsaturated aldehyde.

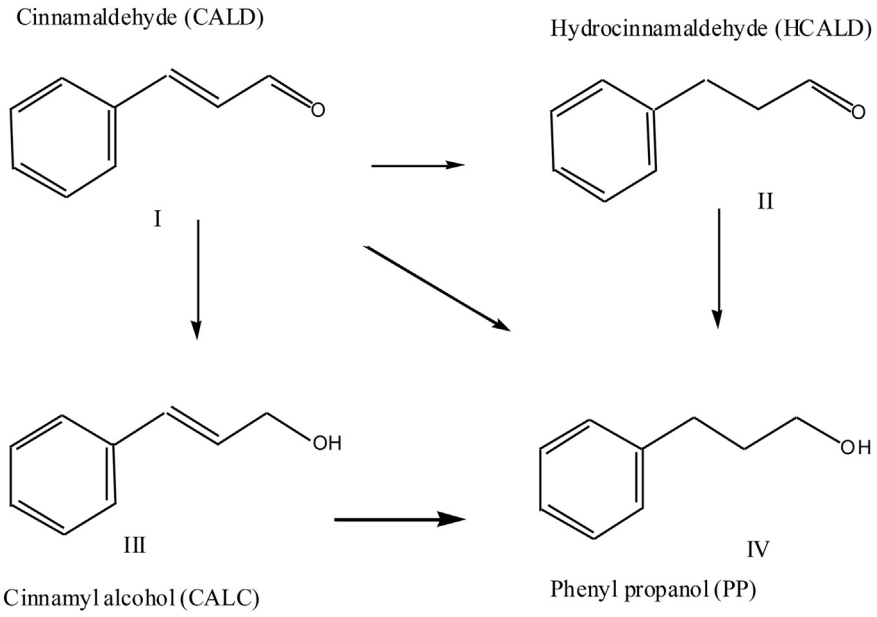

Scheme 3. Reaction pathways in the hydrogenation of cinnamaldhyde.

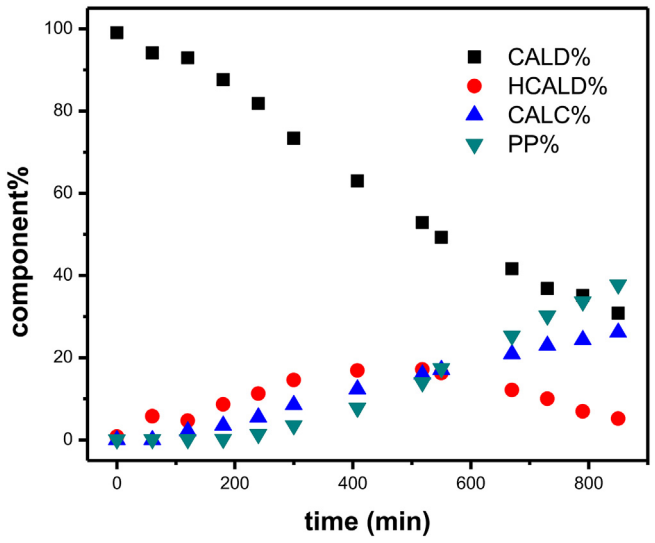

Fig. 10. The progress of the catalytic hydrogenation of cinnamaldehyde: 0.6081 g in 100 mL i-propanol, 0.046 M, Co-catalyst: NaOCH3, 0.0810 g, 1.5 × 10-2 M, Catalyst: complex 1, 0.0424 g, 6.8 × 10-4 M, Temperature: 86 °C, Hydrogen pressure: 4 bar, Reactant: co-cat: cat = 68 : 22: 1.

Declaration of competing interest

The authors declare that they have no known competing financial interests or personal relationships that could have appeared to influence the work reported in this paper.

Acknowledgements

Authors would like to thank the Hashemite University for its research support.

Appendix A. Supplementary data

Supplementary data to this article can be found online at https://doi.org/10.1016/j.molstruc.2020.128327.

References

[1] (a) P.J. Chirik, Acc. Chem. Res. 48 (2015) 1687–1695;
B.L. Small, Acc. Chem. Res. 48 (2015) 2599–2611 (b);
(c) H.A. Younus, N. Ahmad, W. Su, F. Verpoort, Coord. Chem. Rev. 276 (2014) 112–152;
(d) E. Peris, R.H. Crabtree, Chem. Soc. Rev. 47 (2018) 1959–1968.
[2] (a) D. Morales-Morales, C. Jensen, in: The Chemistry of Pincer Ligands, Elsevier, 2007;
(b) G. Van Koten, D. Milstein, Organometallic pincer chemistry, in: Topics in Organometallic Chemistry, vol. 40, Springer-Verlag: Berlin Heidelberg, 2013.
[3] a) S.A. Sahadevan, E. Cadoni, N. Monni, C.S. de Pipaón, J.G. Mascaros, A. Abhervé, N. Avarvari, L. Marchiò, M. Arca, M.L. Mercuri, Cryst. Growth Des. 18 (2018) 4187–4199;
(b) J.S. Derrick, R.A. Kerr, K.J. Korshavn, M.J. McLane, J. Kang, E. Nam, A. Ramamoorthy, B.T. Ruotolo, M.H. Lim, Inorg. Chem. 55 (2016) 5000–5013.
[4] G.K. Rao, W. Pell, I. Korobkov, D. Richeson, Chem. Commun. 52 (2016) 8010–8013;
(b) J.D. Cope, N.P. Liyanage, P.J. Kelley, J.A. Denny, E.J. Valente, C.E. Webster, Chem. Commun. 53 (2017) 9442–9445;
(c) J.A. Therrien, M.O. Wolf, B.O. Patrick, Dalton Trans. 47 (2018) 1827–1840;
(d) T.H.T. Myren, A.M. Lilio, C.G. Huntzinger, J.W. Horstman, T.A. Stinson, T.B. Donadt, Organometallics 38 (2019) 1248–1253.
[5] M. Al-Noaimi, F.F. Awwadi, W.H. Talib, S. Atia, H.H. Hammud, J. Mol. Struct. 1197 (2019) 282–291.
[6] (a) M. Akkoç, S. Demirel, E. Öz, S. Altın, A. Bayri, V. Dorcet, T. Roisnel, C. Bruneau, İ. Özdemir, S. Yaşar, Polyhedron 157 (2019) 434–441;
(b) M. Akkoç, E. Öz, S. Demirel, V. Dorcet, T. Roisnel, A. Bayri, C. Bruneau, S. Altin, S. Yaşar, İ. Özdemir, J. Organomet. Chem. 866 (2018) 214–222.
[7] (a) L. Flamigni, J.P. Collin, J.P. Sauvage, Acc. Chem. Res. 41 (2008) 857–871;
(b) R. Sakamoto, S. Katagiri, H. Maeda, H. Nishihara, Coord. Chem. Rev. 257 (2013) 1493–1506;
(c) C.Y. Wei, Y. He, X.D. Shi, Z.G. Song, Coord. Chem. Rev. 385 (2019) 1–19.
[8] P. Beagley, M.A.L. Blackie, K. Chibale, C. Cailean, J.R. Moss, P.J. Smith, J. Chem. Soc. Dalton Trans. (2002) 4426–4433.
[9] B.L. Tekwami, L.A. Walker, Curr. Opin. Infect. Dis. 19 (2006) 623–631.
[10] J.M. Fritsch, K.A. Thoreson, K. McNeill, J. Chem. Soc. Dalton Trans. (2006) 4814–4820.
[11] J.L. Nowicki, K.S. Johnson, K.H. Coale, V.A. Elord, S.H. Lieberman, Anal. Chem. 66 (1994) 2732–2738.
[12] B. Macias, I. Garcia, M.V. Villa, J. Borras, A. Casiineiras, F. Sanz, Z. Anorg. Allg. Chem. 629 (2003) 255–260.
[13] X.-G. Li, Y.-M. Hua, M.R. Huang, Chem. Eur J. 11 (2005) 4247–4256.
[14] M.H. Lim, B.A. Wong, W.H. Pitcock Jr., D. Mokshagundam, M.-A. Baik, S.J. Lippard, J. Am. Chem. Soc. 128 (2006) 14364–14373.
[15] Y.-H. Kim, J.S. Youk, S.Y. Moon, J.-I. Choe, S.-K. Chang, Chem. Lett. 33 (2004) 702–703.
[16] D. Banerjee, B.C. Mondal, A.K. Das, J. Indian Chem. Soc. 81 (2004) 50–53.

[17] P.K. Bhaumik, A. Bauzá, M.G.B. Drew, A. Frontera, S. Chattopadhyay, CrystEngComm 17 (2015) 5664–5671.
[18] M. Mortoluzzi, G. Paolucci, B. Pitteri, A. Vavasori, Inorg. Chem. Commun. 9 (2006) 1301–1303.
[19] M. Al-Noaimi, O.S. Abdel-Rahman, I.I. Fasfous, M. El-khateeb, F.F. Awwadi, I. Warad, Spectrochim. Acta Part A: Mol. Biomol. Spectrosc. 125 (2014) 375–383.
[20] (a) D. Chatterjee, Coord. Chem. Rev. 252 (2008) 176–198;
(b) M.D. Ward, Coord. Chem. Rev. 250 (2006) 3128–3141;
(c) E. Peris, R.H. Crabtree, Coord. Chem. Rev. 248 (2004) 2239–3246.
[21] R. Drozdzak, B. Allaert, N. Ledoux, I. Dragutan, F. Verpoort, Coord. Chem. Rev. 249 (2005) 3055–3074.
[22] (a) R. Noyori, S. Hashiguchi, Acc. Chem. Res. 30 (1997) 97–102;
(b) H.U. Blaser, B. Pugin, F. Spindler, J. Mol. Catal. A: Chem. 231 (2005) 1–20.
[23] (a) K. Everaere, A. Mortreux, J.F. Carpentier, Adv. Synth. Catal. 345 (2003) 67–77;
(b) J.E. Backvall, J. Organomet. Chem. 652 (2002) 105–111.
[24] M. Al-Noaimi, F.F. Awwadi, W.H. Talib, A. Salem, H.H. Hammud, J. Mol. Struct. 1197 (2019) 282–291.
[25] M. Al-Noaimi, F.F. Awwadi, A. Hammoudeh, S. Abu-Hmaid, R. Bader, Inorganica Chem. Acta (483) (2018) 241–247.
[26] M. Al-Noaimi, A. Hammoudeh, F.F. Awwadi, R. Bader, A. Mahmoud, Inorg. Chem. Acta 471 (2018) 186–193.
[27] M. Al-Noaimi, F.F. Awwadi, A. Hammoudeh, M. Tanash, Transit. Metal Chem. 44 (2019) 355–367.
[28] M. Krejcik, M. Danek, F. Hartl, J. Electroanal. Chem. 317 (1991) 179–187.
[29] C. Nataro, A.N. Campbell, M.A. Ferguson, C.D. Incarvito, A.L. Rheingold, J. Organomet. Chem. 673 (2003) 47–55.
[30] T. Gennett, D.F. Milner, M.J. Weaver, J. Phys. Chem. 89 (1985) 2787–2794.
[31] CrysAlisPro, Agilent Technologies, Version 1.171.35.11 (Release 16–05–2011 CrysAlis171.NET) (Compiled May 16 2011,17:55:39).
[32] SHELXTL (XCIF, XL, XP, XPREP, XS), Bruker AXS Inc., Madison, WI, 2002, version 6.10.
[33] C. Lee, W. Yang, R.G. Parr, Phys. Rev. B 37 (1988) 785–789.
[34] M.J. Frisch et al., Gaussian 09, Revision D.01, Gaussian Inc, Wallingford CT, 2004GaussView3.0, Gaussian: Pittsburgh, PA.
[35] P.J. Hay, W.R. Wadt, J. Chem. Phys. 82 (1985) 270–283.
[36] M.K. Casida, C. Jamorski, K.C. Casida, D.R. Salahub, J. Chem. Phys. 108 (1998) 4439–4449.
[37] R.E. Stratmann, G.E. Scuseria, M.J. Frisch, J. Chem. Phys. 109 (1998) 8218–8224.
[38] M. Cossi, N. Rega, G. Scalmani, V. Barone, Comput. Chem. 24 (2003) 669–681.
[39] N.M. O'Boyle, A.L. Tenderholt, K.M. Langner, J. Comput. Chem. 29 (2008) 839–845.
[40] S.I. Gorelsky, A.B. Lever, M. Ebadi, Coord. Chem. Rev. 230 (2002) 97–105.
[41] D.J. Stufkens, A. Vlček, J. Coord. Chem. Rev. 177 (1998) 127–179.
[42] H.A. Nieuwenhuis, D.J. Stufkens, A. Oskam, Inorg. Chem. 33 (1994) 3212–3217.
[43] B.D. Rossenaar, D.J. Stufkens, A. Vlček, J. Inorg. Chem. 35 (1996) 2902–2909.
[44] K. Abdur-Rashid, S.E. Clapham, A. Hadzovic, J.N. Harvey, A.J. Lough, R.H. Morris, J. Am. Chem. Soc. 24 (2002) 15104–15118.
[45] H.A. Ali, M. Al-Noaimi, S.S. Mahmoud, A.Y. Hammoudeh, Jordan J. Chem. 10 (2015) 58–68.